Core–Shell Nanoparticles

DOI: 10.1002/anie.201408219

# An Upconversion Nanoparticle with Orthogonal Emissions Using Dual NIR Excitations for Controlled Two-Way Photoswitching**

*Jinping Lai, Yixiao Zhang, Nicholas Pasquale, and Ki-Bum Lee**

***Abstract:*** *Developing multicolor upconversion nanoparticles (UCNPs) with the capability of regulating their emission wavelengths in the UV to visible range in response to external stimuli can offer more dynamic platforms for applications in high-resolution bioimaging, multicolor barcoding, and driving multiple important photochemical reactions, such as photoswitching. Here, we have rationally designed single-crystal core–shell-structured UCNPs which are capable of orthogonal UV and visible emissions in response to two distinct NIR excitations at 808 and 980 nm. The orthogonal excitation–emission properties of such UCNPs, as well as their ability to utilize low-power excitation, which attenuates any local heating from the lasers, endows the UCNPs with great potential for applications in materials and biological settings. As a proof of concept, the use of this UCNP for the efficient regulation of the two-way photoswitching of spiropyran by using dual wavelengths of NIR irradiation has been demonstrated.*

Lanthanide-doped upconversion nanoparticles (UCNPs) have recently gained much attention due to their unique capability of upconverting low energy near-infrared (NIR) light to high-energy ultraviolet (UV) and visible light.[1] Combined with other excellent photophysical properties, including long emission lifetimes, narrow emission bandwidths, and high photostability, UCNPs have shown widespread application in fields ranging from bioimaging and sensors to photovoltaics and solid-state devices.[2] One of the critical requirements for harvesting their full potential is to develop UNCPs with emission profiles specifically tuned toward their target applications. This includes synthesizing UCNPs with strong UV emission to trigger chemical reactions such as the photocleavage of photolabile groups,[3] and highly visible emitting UCNPs for nanomedicine-based applications such as photodynamic therapy (PDT),[4] as well as NIR-emitting UCNPs for in vivo bioimaging.[5] Among the various developed UCNPs with tailored emission profiles, multicolor UCNPs capable of regulating their emission wavelengths from the UV to visible range in response to external stimuli are garnering much interest recently, as they can offer more dynamic platforms for applications in high-resolution bioimaging, multicolor encoding, and photoswitching.[6] However, there are only a few reports on such multicolor UCNPs. A typical example is an excitation-responsive UCNP, whose emission can be modulated between spectrally pure visible light and mixed UV/Vis emissions by changing the power density of 980 nm NIR excitation.[6b–d] This unique property of the UNCPs was then successfully applied toward driving important chemical reactions and their subsequent applications such as the two-way photoswitching of dithienylethene,[6b] the reversible control over the reflection of liquid crystals,[6c] and modulating the biocatalytic activity of bacteria.[6d] However, the use of high-power 980 nm NIR light in such UCNP systems, although advantageous, has been shown to cause severe local heating, which has detrimental effects on both solid-state devices and biological systems.[7] Moreover, the spectrally mixed UV/Vis emission of these UCNPs compromises the photoswitching system's ability to reliably encode and transmit information in a spatiotemporally controlled manner. Thus, to overcome these limitations, there is a clear need to develop multicolor UCNPs capable of selectively generating spectrally resolved emissions in the UV and visible regions using external stimuli with negligible heating effects.

We herein describe the design and synthesis of a novel core–shell structured β-$NaYF_4$:$Nd^{3+}$/$Yb^{3+}$/$Tm^{3+}$@$NaYF_4$:$Nd^{3+}$@$NaYF_4$@$NaYF_4$:$Yb^{3+}$/$Er^{3+}$ UCNP (Tm@Er) possessing dual NIR excitations (808 and 980 nm) and the corresponding orthogonal emissions in the UV (347–475 nm)/visible (545 nm) range by using low-power-density excitation for minimal heating effects (Scheme 1). The unique photophysical properties of these UCNPs represent a critical advance in many applications involving the construction of optical storage devices for information storage and transmission, developing advanced drug delivery systems which are capable of the sequential delivery of therapeutics, and multicolor bioimaging and sensing. As a proof-of-concept experiment, we demonstrate the highly efficient two way photoswitching of spiropyran regulated by a single type of UCNP with dual NIR excitations.

The general structure of the UCNP contains a core and multiple shells, including a luminescent core (LC), an internal photon-inert shell (IS), and an outer luminescent shell (LS; Scheme 1 a). In our developed UCNPs, the LC and LS contain different sensitizers and activators to generate orthogonal excitation and emission properties and the IS prevents energy

[*] J. Lai, Y. Zhang,[+] N. Pasquale,[+] K.-B. Lee
Department of Chemistry and Chemical Biology, Rutgers University
Piscataway, NJ 08854 (USA)
E-mail: kblee@rutgers.edu
Homepage: http://kblee.rutgers.edu/

[+] These authors contributed equally to this work.

[**] We acknowledge the kind support from Prof. Riman for fluorescent lifetime measurements. K.-B. Lee acknowledges financial support from the NIH Director's Innovator Award [1DP20D006462-01], the National Institute of Biomedical Imaging and Bioengineering of the NIH [1R21NS085569-01], the N.J. Commission on Spinal Cord grant [09-3085-SCR-E-0], and the Rutgers Faculty Research Grant Program.

Supporting information for this article is available on the WWW under http://dx.doi.org/10.1002/anie.201408219.

  

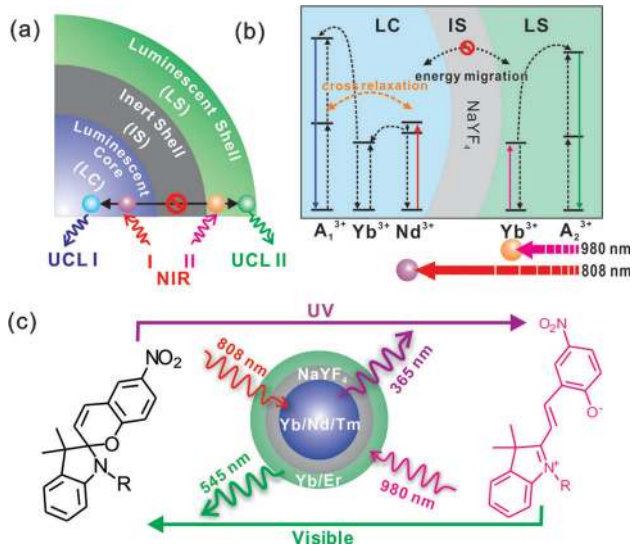


***Scheme 1.*** a) General structural design of the core–shell-structured UCNPs. b) Illustration of the composition of the core–shell UCNPs and the simplified energy level diagram for the photon upconversion under NIR excitations. $Yb^{3+}$ was selectively co-doped with and without $Nd^{3+}$ into the LC and LS as a sensitizer, to endow the LC and LS with an excitation wavelength of 808 nm and 980 nm, respectively. Doping of $Nd^{3+}$ also leads to enhanced cross-relaxation between $Nd^{3+}$ and local activators, which quenches the UCL of the LC and thus endows the LC with a selective excitation of 808 nm with high power density. This structural design leads to orthogonal emissions in the luminescent core–shell under dual NIR excitations. c) Direct and indirect two-way photoswitching of spiropyran by using UV/visible light and using Tm@Er UCNPs with dual NIR excitations.

migration between the two luminescent layers. Following this general design, $NaYF_4$ was chosen as the host matrix because of its low lattice phonon energies and high upconversion efficiency.[1d] We then doped the LS with $Yb^{3+}$ as a sensitizer, while co-doping the LC with both $Nd^{3+}$ and $Yb^{3+}$ (Scheme 1 b). This specific arrangement of sensitizers affords an excitation of 980 nm to the UCNP LS, while the LC is responsive to both 980 nm and 808 nm excitations due to the separate main absorption peaks of $Yb^{3+}$ and $Nd^{3+}$ which locate at 980 and 808 nm, respectively.[8] It should be noted that $Nd^{3+}$ cannot transfer its excitation energy to activators directly. As such, it requires the use of $Yb^{3+}$ as a co-sensitizer, acting as an energy bridge.[8f–h] However, the presence of $Nd^{3+}$ in the LC not only imbues the LC with 808 nm excitation, but also significantly decreases the upconversion luminescence (UCL) of the LC due to the enhanced cross-relaxation between $Nd^{3+}$ and locally positioned activators (quenching effect of $Nd^{3+}$,[8h] for more details see the Supporting Information (SI), Figure S1). As a result, the $Nd^{3+}$-doped LC becomes selectively excited under high-power 808 nm excitation, with no emission observed from low-power 980 nm excitation. Additionally, a layer of $NaYF_4$, without any dopant, was grown in between the LC and LS, as it can serve as a photon inert matrix which prevents energy migration between the LC and LS, which preserves their individual and spectrally pure excitation–emission properties.[9] As such, UCNPs with individual and orthogonal core–shell excitation–emission properties will be achieved, in which the LS and LC will have individual emissions corresponding to individual excitations at 980 nm and 808 nm, respectively. Finally, $Tm^{3+}$ and $Er^{3+}$ were selected as activators of UCL due to their spectroscopic characteristics in the UV and visible region, respectively. In this work, two types of UCNPs were synthesized, henceforth abbreviated as Tm@Er UCNPs and Er@Tm UCNPs. Tm@Er UCNPs have $Tm^{3+}$ doped in the LC and $Er^{3+}$ doped in the LS, displaying UV-blue emission from the LC under 808 nm excitation and green emission from the LS under 980 nm excitation. Er@Tm UCNPs have a reversed core–shell composition with regard to activator doping and therefore reversed emissions. This difference in their emissive properties demonstrates the ability to orthogonally and selectively tune individual emissions based on the choice of activators of UCL (for more details see the main text discussion).

We first synthesized the Tm@Er core–shell UCNPs (Figure 1 a). The UV-blue LC with 808 nm excitation was synthesized according to reported methods.[8g,h] It is comprised of a core (Figure 1 b) doped with $Yb^{3+}$, $Nd^{3+}$, and $Tm^{3+}$, as well as a sensitized shell (Figure 1 c) doped with $Nd^{3+}$ in high concentration. This core–shell structure minimizes the cross-relaxation between $Nd^{3+}$ and the local activators ($Tm^{3+}$) in the core due to the low $Nd^{3+}$ dopant concentration (1 mol %), but maximizes the absorption of 808 nm excitation in the shell due to the high $Nd^{3+}$ concentration (20 %), endowing the nanoparticles with 808 nm excitation at low power density which minimizes local heating effects. As explained previously, to block the energy migration between the LC and LS, a layer of photon-inert $NaYF_4$ was further deposited through epitaxial growth (Figure 1 d). Finally, a green-colored LS, composed of $NaYF_4$:Yb/Er was epitaxially deposited, leading to nanoparticles with a size of 41 ×

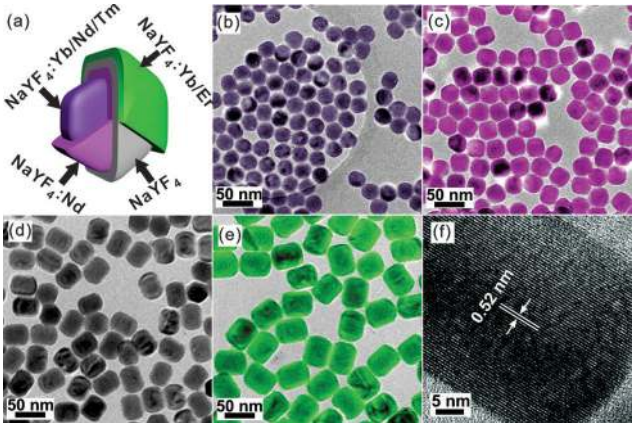


***Figure 1.*** a) Composition of each layer of Tm@Er UCNPs. The false color of each layer represents the corresponding nanoparticles shown in (b–e). b–e) Low-resolution TEM images of Tm@Er UCNPs constructed by epitaxial layer by layer growth. f) High-resolution TEM characterization of a single Tm@Er UCNP. The lattice extending across the particle without interruption is indicative of its monocrystalline structure.

52 nm (width × length, Figure 1e). The shape evolution phenomena during the shell growth of the nanoparticles were ascribed to the kinetically favored anisotropic shell growth during the coating process, which was also observed by other groups.[8i,10] The high-resolution transmission electron microscopy (HRTEM) image shown in Figure 1f shows the (100) crystallographic planes of the Tm@Er UCNPs and demonstrates that the as-synthesized multishell UCNPs were single hexagonal-phase crystals. Additionally, the energy-dispersive X-ray spectroscopy (EDX) spectrum indicates the presence of the elements Na, F, Y, Yb, Nd, Er, and Tm, which confirms the composition of the nanoparticles (see SI, Figure S2).

Next, we studied the upconversion profile of the as-synthesized UCNPs under different wavelength laser excitations. As shown in Figure 2a, the LC of the Tm@Er UCNPs displays the characteristic emission peaks of $Tm^{3+}$ in the UV-blue region when excited using 808 and 980 nm lasers, due to the presence of $Nd^{3+}$ and $Yb^{3+}$ in the luminescent core. Accordingly, a hexane solution of these core nanoparticles displays a deep blue colored band under 808 nm and 980 nm laser irradiation, which is easily seen by the naked eye (Figure 2a, right panel). For Tm@Er, only the characteristic emission peaks of $Tm^{3+}$ can be seen under 808 nm irradiation (Figure 2b, upper curve), demonstrating the selective excitation of LC by 808 nm excitation. In contrast, the UCNPs display strong characteristic emissions from $Er^{3+}$ but relatively weak emissions from $Tm^{3+}$ under 980 nm excitation with a power density of 60 W cm$^{-2}$ (Figure 2b, bottom curve), indicating that both the LC and LS are excited as both of them use $Yb^{3+}$ as sensitizer. It should be noted that the relatively weaker emissions of $Tm^{3+}$ in LC than that of $Er^{3+}$ in LS may be due to 1) the quenching effect of $Nd^{3+}$ in LC,[8h] and 2) the nonlinear excitation nature of UCNPs whereby the UV emissions from $Tm^{3+}$ show a stronger dependence on excitation density than the visible emissions of $Er^{3+}$ (a four photon versus three photon process).[6b] Consequently, decreasing the excitation power density eliminated the $Tm^{3+}$ emissions more quickly than those of $Er^{3+}$, and excitations of 40 W cm$^{-2}$ or lower led to the selective emissions of $Er^{3+}$ in the LS only (Figure 2b, bottom curve). This result demonstrates that the emission of Tm@Er under 980 nm excitation can be easily modulated by regulating the excitation power/wavelength, and that the LS can be selectively excited by utilizing a low excitation power density due to the cooperative effect of the $Nd^{3+}$ doping, the photon-inert shell, and the nonlinear excitation properties of UCNPs,[6b,c,11] as represented in Scheme 1b. Accordingly, a hexane solution of these nanoparticles displays two different colored bands, blue and green, under 808 nm and 980 nm excitation, respectively, with excitation power densities of 40 W cm$^{-2}$ or lower, demonstrating the orthogonal excitation–emission property of the Tm@Er UNCPs. Control experiments demonstrate that UCNPs with the same core–shell structure, but without the critical internal photon-inert shell, display strong energy migration and do not possess separate core–shell excitation–emission properties (Figure S3).

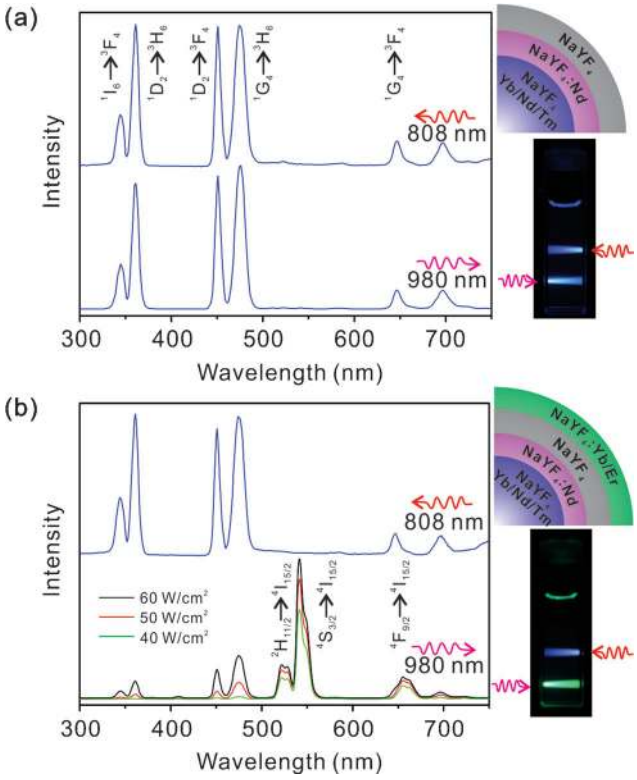


***Figure 2.*** a) Upconversion luminescence profiles of the luminescent core with photon-inert shell and b) the Tm@Er UCNPs under different wavelength excitations and varying power densities. The structures of the corresponding nanoparticles are illustrated in the right panel. The photographs show the UCNPs in hexane solution (1 wt%) under irradiation by two laser beams at wavelengths of 808 nm and 980 nm. The power density for 808 nm and 980 nm lasers is 60 W cm$^{-2}$.

To further demonstrate the rationale behind the structure of the proposed UCNPs, another type of UCNP, Er@Tm, was synthesized based on the inverse composition of the activators $Er^{3+}$ and $Tm^{3+}$ (Figure S4). In contrast to Tm@Er UNCPs, the Er@Tm UNCPs show incomplete separation of the core–shell excitations and emissions. Accordingly, 980 nm laser excitation stimulated not only UV-blue emissions from $Tm^{3+}$ in the LS, but also green emissions from $Er^{3+}$ in the LC (Figure S4f), indicating a simultaneous excitation of the luminescent core and shell by 980 nm irradiation at high power density. The relatively weaker emission from $Er^{3+}$ in the LC is mainly due to the quenching effect of $Nd^{3+}$ on locally placed activators. Decreasing the excitation power density can minimize the emission from $Er^{3+}$, but it will also result in a decrease in UV emission from $Tm^{3+}$ (Figure S5). These results strongly support the rational design of the Tm@Er UCNPs, which have orthogonal core–shell excitation–emission properties at distinct wavelengths to yield spectrally pure UV-blue and green emissions. Furthermore, since 808 nm and low power density 980 nm NIR light both minimize any local heating from the lasers (Figure S6), these UCNPs have unique advantages for applications in materials and biological studies, e.g., for driving important photoreactions with high spatiotemporal control and for reversibly modulating the structure and properties of molecules such as photoswitches, especially for advancing multicolor UCNP-based photoswitching systems which require distinct excita-

  

tion–emission peaks, high photostability, and minimal photoinducible damage.

UCNP-based photoswitching systems, in which UCNPs serve as an antenna and deliver high energy UV/Vis light through the upconversion of low energy NIR light, are capable of the spatiotemporal and reversible modulation of the structure and properties of molecules.[6b,c,g,11] Such systems can overcome the limitations of traditional UV/Vis light-based photoswitching, which include photobleaching, toxicity, and poor penetration through biological tissues. Spiropyran is one of the most studied photoswitchable molecules known to date and is widely used in the development of photoswitches, molecular machines, and sensors.[12] Biomolecules such as nucleic acids, enzymes, cellular receptors, and ion channels have been functionalized with SP to remotely and orthogonally regulate cellular behavior including gene transcription, enzyme activity, and flux through ion channels with light.[13] As illustrated in Scheme 1c, the photoisomerization between spiropyran (SP) and merocyanine (MC) can be regulated by UV and visible light.[12a] Importantly, the maximum absorption peaks of SP and MC that locate at 342 nm and 560 nm, overlap well with the UV emission from the Tm@Er UCNPs under 808 nm excitation and the green emission of our Tm@Er UCNPs under 980 nm excitation, respectively (Figure 3b). As such, we sought to utilize this well-characterized photoswitch in our system to demonstrate the NIR-light-based two-way photoswitching ability of the synthesized Tm@Er UCNPs (Figure 3a).

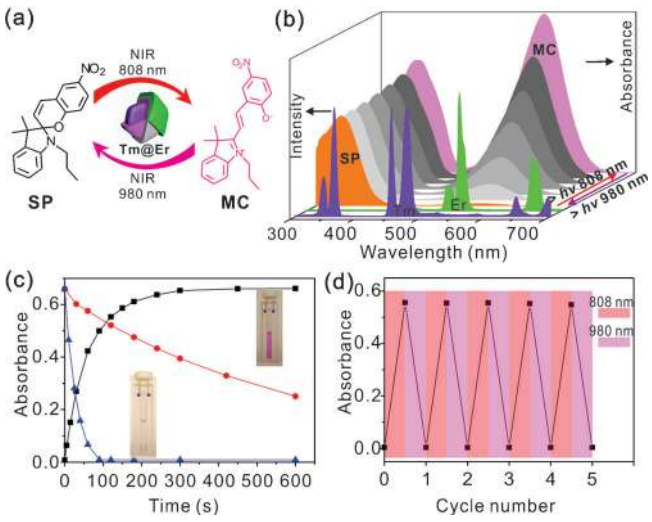


***Figure 3.*** a) Illustration of two-way photoswitching of SP by using Tm@Er UCNPs with dual NIR excitations. b) $Tm^{3+}$ and $Er^{3+}$ emissions from Tm@Er nanoparticles under 808 nm and 980 nm excitations, respectively, which overlap well with the absorption peaks of SP and MC. The evolution of the UV/Vis absorption spectrum of the photoisomerization of SP and MC under 808 nm and 980 nm light irradiation in the presence of Tm@Er UCNPs is shown. c) Kinetic monitoring of the photoswitching reaction of SP and MC under 808 nm and 980 nm light irradiation with Tm@Er UCNPs by using the characteristic absorbance of MC at 560 nm. The red dotted line shows the kinetics of the reaction of MC to SP in the dark. d) Dual NIR light-driven photoswitching of SP over many cycles in THF/methanol (9/1, v/v) solution with 5 wt% of Tm@Er UCNPs and 10 μM of SP by monitoring the absorbance of MC at 560 nm.

The photoswitching of SP by Tm@Er UCNPs was performed with a simple mixture of SP and Tm@Er (for details see Figure S7). As shown in Figure 3b, irradiation of the colorless solution of SP and UCNPs with an 808 nm laser leads to the photoisomerization of SP to MC, resulting in a bright pink solution which is characterized by a red shift in the UV peak as well as a dramatic enhancement of the absorption centered at 560 nm. These results indicate that the ring-opening reaction of the SP to MC was effectively driven by the excitation at 808 nm. Based on the kinetics monitoring of the photoswitching reaction using the characteristic absorption of MC at 560 nm (Figure 3c), 92% of the photostationary state can be obtained within 120 seconds with 808 nm excitation with a power density of 40 $W\,cm^{-2}$. Thereafter, the NIR-light-driven photoisomerization of MC to SP was performed by irradiating the solution with a 980 nm laser. The solution quickly turns back to colorless and the absorption spectrum shows a blue shift in the UV absorption band and a decrease in intensity at 560 nm (Figure 3b). The kinetics of this photoreaction under 980 nm irradiation with Tm@Er UCNPs is much faster than that of the reaction in the dark (Figure 3c). After 980 nm irradiation for 90 seconds with a power density of 15 $W\,cm^{-2}$ the absorption peak of MC no longer exists, indicating a complete photoisomerization reaction of SP to MC. These results demonstrate the successful two-way photoswitching of spiropyran, which is effectively driven using Tm@Er UNCPs with dual NIR excitations at low power density.

We further tested the integrity of SP photoswitching by using Tm@Er UCNPs with low power density 808 nm and 980 nm laser excitations, shown in Figure 3d. A schematic for the "remote control" two-way photoswitching of SP and the Tm@Er UNCPs by using two NIR lasers is shown in Figure 3a. It is worth noting that there is more than 90% retention of SP after five cycles of photoswitching, indicating the robustness and reversibility of our UNCP based photoswitching system, which is mainly due to the attenuation of detrimental heating effects and photobleaching by using NIR light with low excitation power density. Finally, we demonstrated the construction of mesoporous silica-coated Tm@Er (UCNP@MSN), which allow the UCNPs to be easily dispersed in aqueous solutions and undergo facile surface chemistry for further functionalization and application (Figure S8).

In conclusion, we have successfully demonstrated the rational design and preparation of a new type of UCNP, which is capable of producing orthogonal and spectrally pure emissions from core–shell NIR excitations at low power density. In particular, the incorporation of two separate excitation triggers allows for a higher degree of control than achievable using previous systems. Furthermore, in contrast to previously reported photoswitch systems, our system excludes the necessity of high-energy UV/Vis, as well as high-power-density NIR light, which attenuates any system damage from multiphoton absorption and local heating. Taken together, these results demonstrate that both our novel designed UCNP and UCNP-SP-based NIR-driven two-

  

way photoswitching platform has great implications for applications in materials science and biology studies.

Received: August 14, 2014
Revised: September 16, 2014
Published online: October 27, 2014

**Keywords:** core–shell nanoparticles · dual NIR excitations · nanoparticles · two-way photoswitching

[1] a) F. Auzel, *Chem. Rev.* **2004**, *104*, 139; b) S. W. Wu, G. Han, D. J. Milliron, S. Aloni, V. Altoe, D. V. Talapin, B. E. Cohen, P. J. Schuck, *Proc. Natl. Acad. Sci. USA* **2009**, *106*, 10917; c) F. Wang, Y. Han, C. S. Lim, Y. Lu, J. Wang, J. Xu, H. Chen, C. Zhang, M. Hong, X. Liu, *Nature* **2010**, *463*, 1061; d) F. Wang, R. Deng, J. Wang, Q. X. Wang, Y. Han, H. Zhu, X. Chen, X. Liu, *Nat. Mater.* **2011**, *10*, 968; e) F. Wang, X. Liu, *Chem. Soc. Rev.* **2009**, *38*, 976; f) J. Wang, R. Deng, M. A. MacDonald, B. Chen, J. Yuan, F. Wang, D. Chi, T. S. A. Hor, P. Zhang, G. Liu, Y. Han, X. Liu, *Nat. Mater.* **2014**, *13*, 157; g) M. Haase, H. Schafer, *Angew. Chem. Int. Ed.* **2011**, *50*, 5808; *Angew. Chem.* **2011**, *123*, 5928.

[2] a) L. L. Li, P. Wu, K. Hwang, Y. Lu, *J. Am. Chem. Soc.* **2013**, *135*, 2411; b) Y. Zhang, F. Zheng, T. Yang, W. Zhou, Y. Liu, N. Man, L. Zhang, N. Jin, Q. Dou, Y. Zhang, Z. Li, L. P. Wen, *Nat. Mater.* **2012**, *11*, 817; c) R. Deng, X. Xie, M. Vendrell, Y. Chang, X. Liu, *J. Am. Chem. Soc.* **2011**, *133*, 20168; d) H. Gorris, R. Ali, S. M. Saleh, O. S. Wolfbeis, *Adv. Mater.* **2011**, *23*, 1652; e) S. H. Nam, Y. M. Bae, Y. I. Park, J. H. Kim, H. M. Kim, J. S. Choi, K. T. Lee, T. Hyeon, Y. D. Suh, *Angew. Chem. Int. Ed.* **2011**, *50*, 6093; *Angew. Chem.* **2011**, *123*, 6217; f) X. Huang, S. Han, W. Huang, X. Liu, *Chem. Soc. Rev.* **2013**, *42*, 173; g) H. H. Gorris, O. S. Wolfbeis, *Angew. Chem. Int. Ed.* **2013**, *52*, 3584; *Angew. Chem.* **2013**, *125*, 3668; h) L. Sun, Y. Wang, C. Yan, *Acc. Chem. Res.* **2014**, *47*, 1001; i) Y. Yang, Q. Shao, R. Deng, C. Wang, X. Teng, K. Cheng, Z. Cheng, L. Huang, Z. Liu, X. Liu, B. Xing, *Angew. Chem. Int. Ed.* **2012**, *51*, 3125; *Angew. Chem.* **2012**, *124*, 3179; j) Z. Gu, L. Yan, G. Tian, S. Li, Z. Chai, Y. Zhao, *Adv. Mater.* **2013**, *25*, 3758; k) Y. Liu, S. Zhou, D. Tu, Z. Chen, M. Huang, H. Zhu, E. Ma, X. Chen, *J. Am. Chem. Soc.* **2012**, *134*, 15083; l) M. Wang, C. C. Mi, W. X. Wang, C. H. Liu, Y. F. Wu, Z. R. Xu, C. B. Mao, S. K. Xu, *ACS Nano* **2009**, *3*, 1580; m) Q. Liu, Y. Sun, T. Yang, W. Feng, C. Li, F. Li, *J. Am. Chem. Soc.* **2011**, *133*, 17122; n) J. Yang, D. Shen, X. Li, W. Li, Y. Fang, Y. Wei, C. Yao, B. Tu, F. Zhang, D. Zhao, *Chem. Eur. J.* **2012**, *18*, 13642.

[3] a) W. Li, J. Wang, J. Ren, X. Qu, *J. Am. Chem. Soc.* **2014**, *136*, 2248; b) B. Yan, J. C. Boyer, N. R. Branda, Y. Zhao, *J. Am. Chem. Soc.* **2011**, *133*, 19714; c) J. Shen, G. Chen, T. Y. Ohulchanskyy, S. J. Kesseli, S. Buchholz, Z. Li, P. N. Prasad, G. Han, *Small* **2013**, *9*, 3213; d) C. J. Carling, F. Nourmohammadian, J. C. Boyer, N. R. Branda, *Angew. Chem. Int. Ed.* **2010**, *49*, 3782; *Angew. Chem.* **2010**, *122*, 3870.

[4] a) N. M. Idris, M. K. Gnanasammandhan, J. Zhang, P. C. Ho, R. Mahendran, Y. Zhang, *Nat. Med.* **2012**, *18*, 1580; b) S. Cui, D. Yin, Y. Chen, Y. Di, H. Chen, Y. Ma, S. Achilefu, Y. Gu, *ACS Nano* **2013**, *7*, 676; c) X. F. Qiao, J. C. Zhou, J. W. Xiao, Y. F. Wang, L. D. Sun, C. H. Yan, *Nanoscale* **2012**, *4*, 4611; d) C. Wang, L. Cheng, Y. M. Liu, X. J. Wang, X. X. Ma, Z. Y. Deng, Y. G. Li, Z. Liu, *Adv. Funct. Mater.* **2013**, *23*, 3077.

[5] a) G. Chen, T. Y. Ohulchanskyy, R. Kumar, H. Agren, P. N. Prasad, *ACS Nano* **2010**, *4*, 3163; b) N. N. Dong, M. Pedroni, F. Piccinelli, G. Conti, A. Sbarbati, J. E. Ramirez-Hernandez, L. M. Maestro, M. C. Iglesias-de la Cruz, F. Sanz-Rodriguez, A. Juarranz, F. Chen, F. Vetrone, J. A. Capobianco, J. G. Sole, M. Bettinelli, D. Jaque, A. Speghini, *ACS Nano* **2011**, *5*, 8665.

[6] a) J. C. Boyer, C. J. Carling, S. Y. Chua, D. Wilson, B. Johnsen, D. Baillie, N. R. Branda, *Chem. Eur. J.* **2012**, *18*, 3122; b) J. C. Boyer, C. J. Carling, B. D. Gates, N. R. Branda, *J. Am. Chem. Soc.* **2010**, *132*, 15766; c) L. Wang, H. Dong, Y. Li, C. Xue, L. D. Sun, C. H. Yan, Q. Li, *J. Am. Chem. Soc.* **2014**, *136*, 4480; d) Z. Chen, L. Zhou, W. Bing, Z. Zhang, Z. Li, J. Ren, X. Qu, *J. Am. Chem. Soc.* **2014**, *136*, 7498; e) F. Zhang, Q. Shi, Y. Zhang, Y. Shi, K. Ding, D. Zhao, G. D. Stucky, *Adv. Mater.* **2011**, *23*, 3775; f) C. Zhang, C. H. Xu, L. D. Sun, C. H. Yan, *Chem. Asian J.* **2012**, *7*, 2225; g) B. F. Zhang, M. Frigoli, F. Angiuli, F. Vetrone, J. A. Capobianco, *Chem. Commun.* **2012**, *48*, 7244.

[7] a) Q. Zhan, J. Qian, H. Liang, G. Somesfalean, D. Wang, S. He, Z. Zhang, S. Andersson-Engels, *ACS Nano* **2011**, *5*, 3744; b) Z. Jiang, M. Xu, F. Li, Y. Yu, *J. Am. Chem. Soc.* **2013**, *135*, 16446.

[8] a) J. Qiu, Y. Kawamoto, *J. Appl. Phys.* **2002**, *91*, 954; b) L. C. Courrol, I. M. Ranieri, L. V. G. Tarelho, S. L. Baldochi, L. Gomes, N. D. Vieira, *J. Appl. Phys.* **2005**, *98*, 113504; c) Y. L. Huang, K. H. Jang, H. J. Seo, K. W. Jang, *J. Appl. Phys* **2006**, *100*, 083513; d) C. Koepke, K. Wisniewski, L. Sikorski, D. Piatkowski, K. Kowalska, M. Naftaly, *Opt. Mater.* **2006**, *28*, 129; e) A. Lupei, V. Lupei, C. Gheorghe, A. Ikesue, E. Osiac, *Opt. Mater.* **2009**, *31*, 744; f) Y. F. Wang, G. Y. Liu, L. D. Sun, J. W. Xiao, J. C. Zhou, C. H. Yan, *ACS Nano* **2013**, *7*, 7200; g) X. Xie, N. Gao, R. Deng, Q. Sun, Q. Xu, X. Liu, *J. Am. Chem. Soc.* **2013**, *135*, 12608; h) J. Shen, G. Y. Chen, A. M. Vu, W. Fan, O. S. Bilsel, C. C. Chang, G. Han, *Adv. Opt. Mater.* **2013**, *1*, 644; i) H. Wen, H. Zhu, X. Chen, T. F. Hung, B. Wang, G. Zhu, S. F. Yu, F. Wang, *Angew. Chem. Int. Ed.* **2013**, *52*, 13419; *Angew. Chem.* **2013**, *125*, 13661.

[9] Q. Su, S. Han, X. Xie, H. Zhu, H. Chen, C. Chen, R. Liu, X. Chen, F. Wang, X. Liu, *J. Am. Chem. Soc.* **2012**, *134*, 20849.

[10] a) K. A. Abel, J. C. Boyer, C. M. Andrei, F. C. J. M. van Veggel, *J. Phys. Chem. Lett.* **2011**, *2*, 185; b) C. Zhang, J. Y. Lee, *ACS Nano* **2013**, *7*, 4393.

[11] J. Liu, W. Bu, L. Pan, J. Shi, *Angew. Chem. Int. Ed.* **2013**, *52*, 4375; *Angew. Chem.* **2013**, *125*, 4471.

[12] a) R. Klajn, *Chem. Soc. Rev.* **2014**, *43*, 148; b) V. I. Minkin, *Chem. Rev.* **2004**, *104*, 2751.

[13] a) T. Sakata, Y. L. Yan, G. Marriott, *Proc. Natl. Acad. Sci. USA* **2005**, *102*, 4759; b) Y. Ito, N. Sugimura, O. H. Kwon, Y. Imanishi, *Nat. Biotechnol.* **1999**, *17*, 73; c) C. Beyer, H. A. Wagenknecht, *Synlett* **2010**, 1371; d) A. Kocer, M. Walko, W. Meijberg, B. L. Feringa, *Science* **2005**, *309*, 755.

  